EDGE ARTICLE

A new type of noncovalent surface–π stacking interaction occurring on peroxide-modified titania nanosheets driven by vertical π-state polarization†

Shenqian Ma,[a] Weixin Zhao,[a] Jun Zhou,[a] Jiaou Wang,[b] Shengqi Chu,[b] Zigeng Liu [ID][c] and Guolei Xiang [ID] *[a]

Noncovalent π stacking of aromatic molecules is a universal form of noncovalent interactions normally occurring on planar structures (such as aromatic molecules and graphene) based on sp²-hybridized atoms. Here we reveal a new type of noncovalent surface–π stacking unusually occurring between aromatic groups and peroxide-modified titania (PMT) nanosheets, which can drive versatile aromatic adsorptions. We experimentally explore the underlying electronic-level origin by probing the perturbed changes of unoccupied Ti 3d states with near-edge X-ray absorption fine structures (NEXAFS), and find that aromatic groups can vertically attract π electrons in the surface peroxo-Ti states and increase their delocalization regions. Our discovery updates the concept of noncovalent π-stacking interactions by extending the substrates from carbon-based structures to a transition metal oxide, and presents an approach to exploit the surface chemistry of nanomaterials based on noncovalent interactions.

Introduction

Atomically-thin two-dimensional (2D) materials can widely display unusual physical and chemical properties due to the minimized lattice confinements on electronic structures and maximized specific surface areas.[1,2] The least-confined electronic states can intrinsically modify their properties and enhance the bonding abilities of surface atoms; the largest specific surface area can extremely increase the available surface sites for chemical interactions, and enlarge the effects of surface chemical states on tuning physical and chemical properties.[3,4] These structural features make 2D materials ideal platforms to explore the applications and mechanisms of heterogeneous catalysis, electrocatalysis, single-atom catalysis, confinement effects, *etc.*[1–3,5] To date, many 2D materials have been prepared and explored as catalysts and supports;[6–13] however, few studies focus on their noncovalent interactions, particularly the cases with aromatic molecules.[14] Moreover, due to the limits of material models and characterization strategies, it has long remained challenging to experimentally probe the electronic mechanisms driving the surface interactions of most

materials.[15,16] Thus the physicochemical nature of many nanoscale phenomena has long remained mysterious. Hence, to deeply reveal the features and electronic principles of nanosurface chemistry, ideal model systems based on appropriate 2D materials and chemical interactions still need to be widely explored.

Titania contains a group of titanium oxides that have been widely used as catalytic supports, photocatalysts, photovoltaic materials, and substrates in surface sciences.[17–20] Their energy band states and orbital-level interaction mechanisms with adsorbates can be revealed by probing the varied signals of the Ti-L₃ line with near edge X-ray absorption fine structure (NEXAFS), a technology that detects the densities of unoccupied electronic states.[15,18] Thus 2D titania nanosheets are appropriate model systems to explore new properties and fundamental issues in nanosurface chemistry.[4,21] For example, ultrathin 2D titania has been widely explored in photocatalysis,[22,23] single-atom catalysis,[24] surface enhanced Raman spectroscopy (SERS),[25] surface modifications, and ligand-induced surface effects.[15,26]

Herein, using 2D titania as a model platform, we reveal a new type of noncovalent surface–π interaction occurring between aromatic groups and peroxide-modified titania (PMT) nanosheets. The oxide substrate of this new aromatic interaction is different from those of traditional π–π and surface–π interactions occurring on planar structures basically derived from sp²-hybridized carbon atoms. We refer to this new type of noncovalent surface–aromatic stacking interaction as PMT–aromatic interaction. The underlying electronic mechanism can be experimentally revealed with NEXAFS through probing the

[a]State Key Laboratory of Chemical Resource Engineering, College of Chemistry, Beijing University of Chemical Technology, Beijing 100029, China. E-mail: xianggl@mail.buct.edu.cn; sinbool@qq.com

[b]Beijing Synchrotron Radiation Facility, Institute of High Energy Physics, Chinese Academy of Science, Beijing 100049, China

[c]Forschungszentrum Jülich GmbH, Institute of Energy and Climate Research Fundamental Electrochemistry (IEK-9), Jülich, 52425, Germany

bonding states of surface Ti 3d orbitals. We discover that π electrons in surface π states can be vertically polarized towards aromatic groups, which decreases the filling degree of Ti 3d orbitals but increases the total delocalization of π electrons. This is the intrinsic electronic-level driving force underlying this new type of noncovalent surface–π interaction.

Results and discussion

Aromatic adsorption on peroxide-modified titania (PMT)

We discover the nature of this untraditional noncovalent surface–π interaction from understanding why PMT materials can versatilely adsorb aromatic molecules.[26] In this research the primary PMT model is prepared by hydrolyzing peroxo-Ti precursors in H_2O (see details in Methods). Basically, this material is composed of wrinkled nanosheets as shown by transmission electron microscopy (TEM) images (Fig. 1a, S1a and b†). The wrinkled morphology challenges direct measurement of the thickness with atomic force microscopy (AFM), and thus we alternatively determine the thickness by imaging their edges with TEM, which is about 1.0 nm as shown in Fig. 1a.[21,27,28] The BET surface area of the PMT nanosheets determined with multipoint N_2 adsorption is 204.4 m^2 g^{-1} (Fig. S1c and d†).

The PMT nanosheets can separate Rhodamine B (RhB), a red cationic dye (see Fig. 1b), from an aqueous solution of 0.20 mmol L^{-1} through natural settling (Fig. 1c). However, peroxide-free titania (PFT) nanosheets (Fig. S1e†), which are prepared by removing peroxide ligands through ligand exchange with OH^- in 1.0 mol L^{-1} NaOH solution, cannot adsorb RhB. Nevertheless, the adsorption capability can be recovered by re-adsorbing peroxide ligands (Fig. 1c). Likewise, raw TiO_2(B) nanosheets (Fig. S2a†), prepared by hydrolyzing $TiCl_4$ in ethylene glycol, cannot adsorb RhB either,[22] but become active after peroxide modification (Fig. S2b†). The BET surface area of PFT nanosheets is 204.3 m^2 g^{-1} (Fig. S1f†). These results indicate that such adsorptions on titania nanosheets critically result from surface modification by peroxides, but do not directly depend on crystal structures, exposed facets and surface area. We find that TiO_2 nanoparticles cannot adsorb RhB in the presence of H_2O_2 (Fig. S2c and d†), because their surfaces cannot be effectively modified by peroxide ligands due to reduced surface reactivity. These visible adsorptions depending on surface modification states motivate us to deeply explore the feature and origin of this phenomenon.

In addition to dyes, we further find that PMT can also adsorb other types of aromatic molecules, such as tryptophan (Trp), indole (Ind), 2-methylindole (Min), cinnamyl alcohol (CAL), benzyl alcohol (BAL), phenyl propanol (PPL) and benzoic acid (BA) (see Fig. 1b). Fig. 1d and S3–S5† present concentration-dependent equilibrium adsorptions (n_e) of RhB, Trp and BA by 40.0 mg of PMT and PFT at 25 °C, in which different amounts of aromatic molecules (n_0) are dissolved in 8.0 mL of water at pH = 7.0. Fig. 1e and S6a–h† show instantaneous adsorption
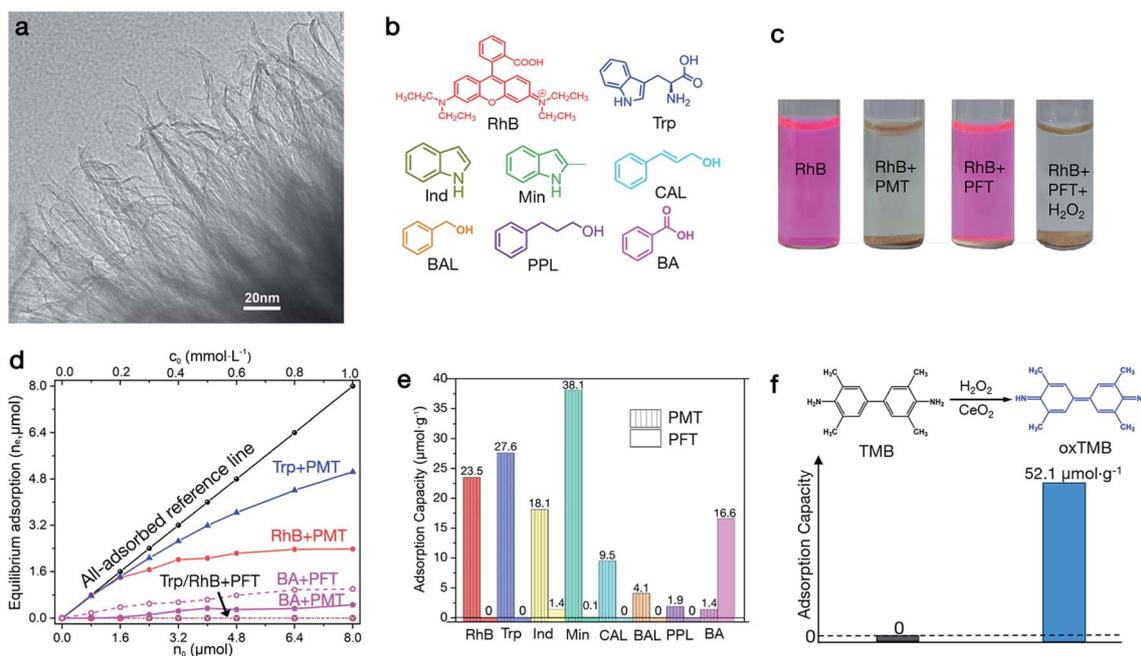

Fig. 1 Adsorptions of aromatic molecules on peroxide-modified titania (PMT) nanosheets driven by PMT−aromatic interaction. (a) TEM image of PMT nanosheets showing their 2D morphology and wrinkled edges. (b) Aromatic molecules used to reveal PMT−aromatic interaction, including Rhodamine B (RhB), tryptophan (Trp), indole (Ind), 2-methylindole (Min), cinnamyl alcohol (CAL), benzyl alcohol (BAL), phenyl propanol (PPL) and benzoic acid (BA). (c) Results for separation of RhB in water by PMT, peroxide-free titania (PFT), and remodified PFT by H_2O_2 through natural settling. (d) Concentration-dependent equilibrium adsorption capacities (n_e) of RhB, Trp and BA by 40.0 mg of PMT (solid lines) and PFT (dashed lines) at varied initial concentrations (n_0). (e) Instantaneous adsorption capacities (n_i) of aromatic molecules on PMT and PFT. (f) The varied saturated adsorption capacities of TMB and oxidized TMB (oxTMB) on PMT.

capacities (n_i) of RhB, Trp, Ind, Min, CAL, BAL, PPL and BA in 8.0 mL of 0.20 mmol L^{-1} solution on PMT and PFT. The equilibrium adsorptions are performed for 30 min, which more reflects the thermodynamic feature of aromatic–PMT interaction; while instantaneous adsorptions are performed for 1 min, which more indicates kinetics properties. At low concentrations (<0.20 mmol L^{-1}), RhB and Trp are all adsorbed by 40.0 mg of PMT, and the equilibrium adsorption increased with concentration until saturation (Fig. 1d). However, PFT cannot adsorb RhB and Trp at all concentrations. The instantaneous adsorptions of RhB and Trp on PMT are 23.5 and 27.6 μmol g^{-1}, but both are zero on PFT (Fig. 1e). Ind and Min can also be effectively adsorbed by PMT but weakly by PFT, as indicated by their instantaneous adsorption ratios of 18.1 : 1.4 and 38.1 : 0.1. CAL, BAL and PPL show the same adsorption trends as RhB and Trp, whose instantaneous adsorptions are 9.5, 4.1 and 1.9 μmol g^{-1} on PMT and all are zero on PFT (Fig. 1e). These results further indicate that PMT can widely adsorb aromatic molecules, but this attractive PMT–aromatic interaction is critically controlled by surface peroxide ligands. The critical roles of peroxide ligands lead to monolayer aromatic adsorptions, which can be confirmed by the Langmuir-type adsorptions determined by fitting the adsorption isotherms (Fig. S7†).

Feature and driving forces of PMT–aromatic interaction

Such PMT–aromatic interactions are driven by physisorption. First, this can be supported by the different adsorption trends of BA from those of other aromatic molecules. The –COOH group conjugated to benzene is a strong ligand, and thus BA adsorbs on PFT through chemisorption, which is competitively inhibited by chemisorbed peroxide ligands. Our results show that the adsorption capacity of BA on PFT is greater than that on PMT at all concentrations (Fig. 1d and S5†), and its instantaneous adsorption decreases from 16.6 to 1.4 μmol g^{-1} (Fig. 1e). The difference indicates that PMT adsorbs the other aromatic molecules (RhB, Trp, CAL, BAL and PPL) through physisorption, otherwise, their instantaneous adsorptions should also be greater on PFT. When –COOH is not conjugated to aromatic groups, it shows lower coordination activity. For example, the instantaneous adsorption of 2-phenylpropionic acid on PFT is 0 μmol g^{-1}, while the capacity is 6.2 μmol g^{-1} on PMT (Fig. S6i†), which shows the same trend as RhB and Trp. RhB and Trp molecules also contain COOH groups, but their adsorptions are dominated by physisorption. The bonding capability of –COOH in RhB may be reduced by the steric hindrance, and the bonding capabilities of the –COOH group in Trp may be reduced by the –NH$_2$ group. Second, the strong adsorptions of Ind and Min on PMT exclude the necessary contributions of chemisorption (Fig. 1e and S6†). Ind and Min have no functional groups to form chemisorption, and thus their adsorptions on PMT can only be driven by physisorption.

This PMT–aromatic interaction specifically occurs between aromatic groups and PMT. At pH = 7.0, both PFT and PMT are negatively charged as indicated by their zeta potentials (Table S1†), and RhB is positively charged as a cationic dye. The zero adsorption of RhB on PFT excludes the dominant role of electrostatic attraction. The adsorptions of neutrally charged Ind, Min, CAL, BAL and PPL on PMT further eliminate the roles of electrostatic interactions. In addition, because RhB and Trp are adsorbed from aqueous solutions and water molecules show strong hydrogen bonds, hydrogen bonds cannot drive such PMT–aromatic attractions. Furthermore, as surface peroxide groups are removed on PFT by washing PMT with NaOH solution, more –OH groups should appear on PFT than on PMT. The result that PFT cannot adsorb aromatic molecules indicates that surface –OH groups cannot induce the adsorption phenomenon. Therefore, aromatic groups should play critical roles.

To further verify the dominant roles of aromatic groups, we used TMB (3,3′,5,5′-tetramethylbenzidine, Fig. 1f), a chromogenic reagent upon oxidation, as a model molecule to vary conjugated aromatic size. We find that TMB cannot be adsorbed by PMT nanosheets but ox-TMB can be adsorbed (Fig. 1f and S8†), and the saturated adsorption capacity is 52.1 μmol g^{-1}. TMB cannot be adsorbed by PMT due to the small size of the benzene ring, while the aromatic size of oxidized TMB (ox-TMB) is increased due to the conjugation of benzene rings through the –C=C– bond.[29] Such a dramatically enhanced adsorption capacity indicates the critical roles of aromatic groups in generating this unusual PMT–aromatic interaction. In addition, the greater adsorption capacity of CAL than PPL also indicates the effects of aromatic size. In CAL, the benzene ring conjugates with the –C=C– bond, which leads to a larger π system than the benzene ring in PPL.

This aromatic–PMT interaction is stronger than normal π–π stackings. The attractive noncovalent interactions in the system typically involve heterogeneous aromatic-surface force (F_{as}), homogeneous solvation force (F_s) applied to the molecules and intermolecular forces (F_i) mainly through π–π stacking. RhB and Trp can form stable dilute solutions of 40.0 μmol L^{-1} in water, thus $F_s > F_i$; the effective separations by PMT indicate that $F_{as} > F_s$. Then the strength order of the forces follows $F_{as} > F_s > F_i$, meaning that the PMT–aromatic interaction is even stronger than normal π–π stackings for RhB and Trp. As a result, the factors that can affect the strengths of these forces, such as aromatic size, the polarity of solvent, pH of solutions, configurations of molecules, functional groups and charging states of surfaces and adsorbate molecules, can affect the adsorption capacities.

Difference of PMT–aromatic from normal surface–π interactions

The difference of PMT–aromatic interaction from traditional surface–π attractions lies in the substrate (Fig. 2). Normal surface–π interactions usually occur on graphene-derived carbon materials, which display delocalized Π_∞^∞ electronic states combined with $2p_z$ orbitals perpendicular to the atomic planes.[30,31] The nature of such interactions is extended π–π stackings. In contrast, PMT–aromatic interaction occurs on peroxide-modified titania nanosheets. Oxides do not intrinsically display delocalized Π_∞^∞ electronic states as graphene, and thus PMT–aromatic interaction extends the form of π-stacking interactions from sp²-hybridized planar structures to
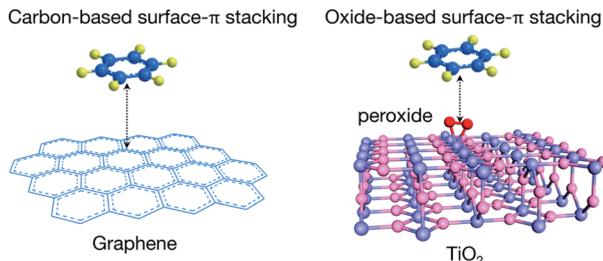
Fig. 2 Scheme illustrating the different substrates of traditional surface–π interactions with graphene-based materials and PMT–aromatic interaction.
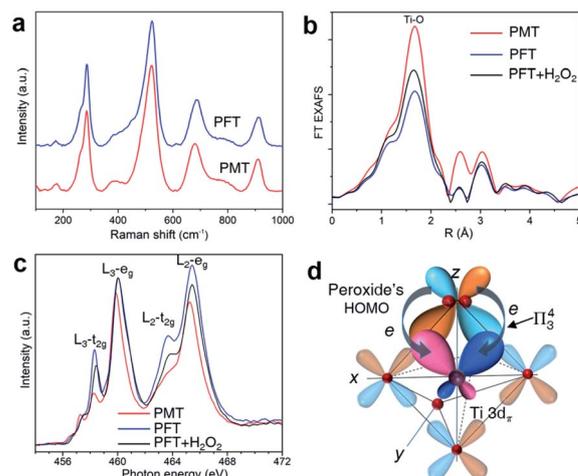

Fig. 3 Probing the bonding states of peroxide ligands on PMT. (a) Raman spectra showing the unchanged crystal structures of PMT and PFT. (b) R-Space EXAFS data indicating that peroxide modification increases the coordination number of Ti atoms. (c) NEXAFS results of the Ti $L_{2,3}$-edge revealing the orbital interactions of peroxide with surface Ti 3d orbitals. (d) Scheme demonstrating the orbital overlap of peroxide's π*-type HOMOs with Ti $3d_\pi$ orbitals and the formation of Π_3^4 centers.

a transition metal oxide. Moreover, for traditional π–π and surface–π interactions, it is challenging to experimentally probe their electronic mechanisms, and thus their origins have been mainly studied through simulations.[32,33]

Several simulation strategies and concepts have been proposed to understand the nature of intermolecular π–π stacking interactions, such as the electrostatic quadrupole π–σ attraction model,[34] electrostatic potential surfaces,[35] local substituent effects in π-stackings,[33,36] dispersion-driven π-stackings,[31,37] collective charge fluctuations,[38] etc. However, the electronic origins of π stackings are still highly under debate due to the lack of direct experimental support.[38,39] In our system, the bonding states of Ti 3d orbitals can be detected with NEXAFS, which enables experimentally probing the atomic and electronic mechanisms of how aromatic molecules interact with PMT.

Atomic and electronic interactions of peroxide ligands with titania

Atomically, peroxide ligands bond to surface Ti atoms through bidentate ligation. Peroxide ligands do not change the crystal structures of PMT and PFT nanosheets, as shown by Raman spectra (Fig. 3a) and XRD patterns (Fig. S1b†). The R-space results of Ti K-edge extended X-ray absorption fine structures (EXAFS, Fig. 3b and S9†) display varied intensities of the Ti–O peak at 0.16 nm, which means that peroxide modification can increase the coordination numbers of surface Ti atoms.

Electronically, peroxide ligands increase the delocalization volumes of π electrons through overlapping their highest occupied molecular orbitals (HOMOs) with π-type 3d ($3d_\pi$) orbitals of surface Ti atoms. We analyze the underlying electronic interactions with the Ti-L_3 absorption edge that arises from dipole electron transition from the core-level $2p_{3/2}$ state to unoccupied 3d character in t_{2g} and e_g states. In contrast, the higher Ti-L_2 edge is rarely analyzed, because the concurrent excitation of $2p_{1/2}$ and $2p_{3/2}$ electrons complicates the curves.[18] For atomically thin titania nanosheets, ligand-induced changes in peak widths and intensities of Ti-L_3 lines can reveal the bonding features of surface Ti atoms.[15] PMT shows the lowest Ti-L_3 t_{2g} and the narrowest e_g peaks, while PFT shows higher L_3-t_{2g} and broader L_3-e_g peaks (Fig. 3c). This difference reveals that peroxide ligands can suppress the extensions of both $3d_\pi$ (d_{xz} and d_{yz}) and $3d_\sigma$ (d_{z^2}) orbitals of surface Ti atoms into lattice

Bloch states. Instead, these orbitals are redistributed into the surface coordination bonds with peroxide ligands. After re-modifying PFT with H_2O_2, the Ti-L_3 t_{2g} peak decreases but the Ti-L_3 e_g peak remains unchanged, indicating that the π*-type HOMOs of peroxide ligands mainly overlap with the $3d_\pi$ orbitals of surface Ti atoms, which is basically driven by their matched phase symmetries (Fig. 3d). In the spectra, the L_3-e_g peaks of PFT with or without H_2O_2 treatments show the same widths, while PMT's L_3-e_g peak is narrower. This is because PMT was prepared by directly hydrolyzing $TiCl_3$ in H_2O_2 solutions, and peroxide appears both on the surfaces and in the lattices. Peroxides can be removed through washing with NaOH solutions, but some still remain in the lattice, as shown by the O 1s peaks of X-ray photoelectron spectra (XPS, Fig. S10†). Removal of surface peroxide ligands leads to increased L_3-t_{2g} from PMT to PFT, while the widened L_3-e_g mainly results from part removal of lattice peroxides. Re-adsorbed peroxides mainly bond to surface Ti atoms of PFT, but cannot embed into lattice sites. Thus, re-modifying PFT with H_2O_2 mainly decreases L_3-t_{2g}, while L_3-e_g remains unchanged. This further indicates that surface peroxide ligands specifically modify the filling degrees of t_{2g} states through π bonds.

To form the π-type surface coordination bond, peroxide must act as a bidentate ligand to form an η^2-O_2–Ti configuration as shown in Fig. 2, which is consistent with the bonding structure of peroxide with transition metals.[40] Then the degenerate peroxide's HOMOs can share their electron pairs with Ti $3d_\pi$ orbitals through this coordination bond, which yields localized Π_3^4 centers. As a result, for peroxide, the delocalization volumes of its π electrons, the conjugation region and polarizability of π states are increased due to the formation of such π-type surface complexes.

Electronic origin of PMT–aromatic interaction

We use Trp as a probe to reveal how aromatic groups interact with PMT. The unchanged R-space EXAFS data within 1.0–6.0 Å suggest that adsorbed aromatic molecules neither eliminate surface peroxide ligands, nor change the coordination states of Ti atoms (Fig. 4a and S9a†). Nuclear magnetic resonance (NMR) results show that the molecular structures of desorbed Trp are not changed (Fig. S11†). These results further confirm the noncovalent adsorption nature of aromatic molecules on PMT. Furthermore, Trp and Ind do not absorb visible light in solutions and mixtures with PFT or H_2O_2 (Fig. 4b and S11d†). However, both show similar and strong absorption modes between 400 and 800 nm after being adsorbed on PMT. This means that noncovalent PMT–aromatic interaction can modify the optical properties and electronic structures of aromatic molecules.

NEXAFS results reveal that noncovalent PMT–aromatic attraction can redistribute the delocalization states of π electrons in PMT's Π_3^4 surface states. Fig. 4c shows the comparison of the Ti-$L_{2,3}$ lines of PMT, PFT and Trp–PMT. From PFT to PMT, peroxide ligands share electrons with Ti $3d_\pi$ orbitals through η^2-O_2–Ti bonds, which decreases the densities of unoccupied $3d_\pi$ states and leads to a reduced t_{2g} peak. Different from the results of removing surface peroxide ligands from PMT, however, noncovalently-adsorbed Trp molecules on PMT just selectively enhance the t_{2g} peak, but have no influence on the e_g state. The results mean that Trp molecules only decrease the filling degrees of $3d_\pi$ orbitals, indicating that electronic interactions can occur between aromatic states and surface Π_3^4 states. Moreover, the lower t_{2g} intensity of Trp–PMT than PFT indicates that η^2-O_2–Ti bonds are not broken, which is consistent with the unchanged coordination states of Ti atoms

Fig. 5 Aromatic recycling by a PMT membrane visually illustrated with RhB. (a) PMT membrane on filter paper prepared by filtration. (b) SEM image of the PMT membrane. (c) RhB adsorption from water *via* filtration. (d) RhB release triggered by NaOH solution.

as shown in Fig. 4a. Therefore, the electronic picture of the noncovalent PMT–aromatic attraction is that, peroxide's π electrons delocalized in surface Π_3^4 states of PMT are further redistributed towards aromatic groups (Fig. 4d). The result also indicates that such a vertical delocalization only polarizes π states to a limited extent, but cannot lead to orbital overlapping and electron sharing. The vertically polarized π states can also increase the delocalization volumes of π electrons and decrease the total energy, which differs from the normal lateral approach through covalently overlapping more sp^2-hybridized p_z orbitals.

Application of PMT–aromatic interaction in dye recycling

This ligation-induced aromatic interaction can be switched on/off by varying surface ligation states, and thus can be used to separate and recycle aromatic compounds from solutions. We use RhB as a model compound to visually demonstrate such applications through filtration by a PMT membrane (Fig. 5 and Video S1†). The PMT membrane is prepared by depositing PMT through filtration (Fig. 5a). The scanning electron microscopy image (SEM, Fig. 5b) shows that the membrane is porous and composed of aggregated microscale particles by PMT nanosheets on the micrometer scale. Video S1† and Fig. 5c visually display that RhB molecules can be effectively separated from aqueous solution. After separation, RhB molecules are all adsorbed by the membrane, but can be further released after removing surface peroxide ligands through elution with NaOH solution (Fig. 5d).

Conclusions

In summary, we have revealed a new type of noncovalent surface–π attraction interaction occurring between aromatic
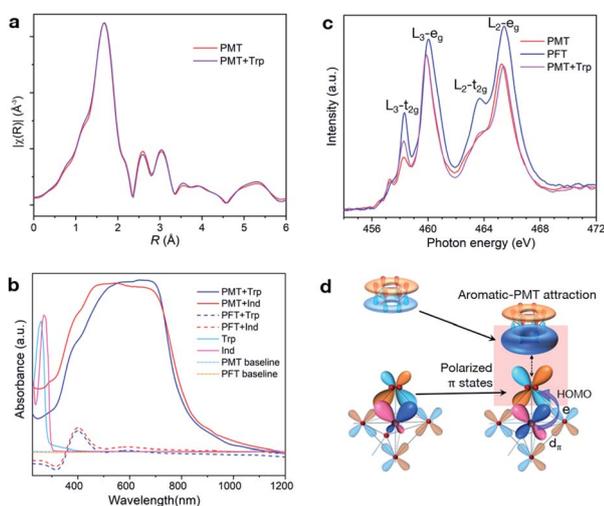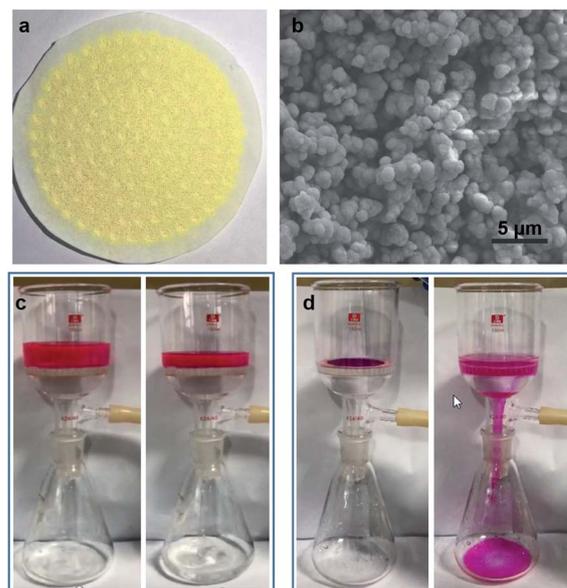

Fig. 4 Revealing electronic-level interaction mechanisms of aromatic groups with PMT. (a) R-Space EXAFS data of Ti K-edge characterizing the adsorption state of Trp on PMT. (b) Adsorption-induced optical absorption modes of Trp and indole (Ind) on PMT in the visible region. (c) NEXAFS of the Ti $L_{2,3}$-edge characterizing the electronic interaction mechanisms of Trp with PMT. (d) Scheme illustrating orbital polarizations towards the contacting region that drives the noncovalent PMT–aromatic attraction.

groups and peroxide-modified titania nanosheets. This unusual PMT–aromatic interaction extends the concept of π stackings from graphene-based materials to a transition metal oxide, and expands the family of noncovalent π interactions already containing π–π, cation–π, anion–π, and XH–π interactions. This PMT–aromatic interaction primarily results from the modification of surface Ti sites by peroxide ligands, while other factors such as size and surface area can affect the surface reactivity, and further affect the adsorption performances. We anticipate that this interaction mode inspires future exploitations of 2D materials in adsorption, separation, catalysis, supramolecular chemistry, biochemistry and materials science based on noncovalent interactions.

We also experimentally reveal through NEXAFS that the PMT–aromatic interaction electronically results from vertical π-state polarizations between aromatic groups and PMT. This electronic interaction mode may be a common intrinsic property of π states, and a general mechanism underlying noncovalent π interactions. This is an example illustrating how to use 2D materials as ideal model systems to explore the electronic-level mechanisms of surface chemical interactions. More calculation methods need to be further developed to explore new types of surface–aromatic interactions and the electronic features of aromatic groups in noncovalent π interactions.

Author contributions

G. X. initiated and conceived the research, designed the experiments and wrote the manuscript. S. M. and G. X. carried out the experiments. S. M., G. X., J. W. and S. C. carried out XAFS measurements, and G. X. analysed the results. W. Z. and J. Z. helped with the experiments. Z. L. contributed to designing the research. All authors commented on the manuscript.

Conflicts of interest

There are no conflicts to declare.

Acknowledgements

Notes and references

1 Y. Wang, J. Mao, X. G. Meng, L. Yu, D. H. Deng and X. H. Bao, *Chem. Rev.*, 2019, **119**, 1806–1854.
2 Y. F. Sun, S. Gao, F. C. Lei and Y. Xie, *Chem. Soc. Rev.*, 2015, **44**, 623–636.
3 M. Chhowalla, H. S. Shin, G. Eda, L. J. Li, K. P. Loh and H. Zhang, *Nat. Chem.*, 2013, **5**, 263–275.
4 D. H. Deng, K. S. Novoselov, Q. Fu, N. F. Zheng, Z. Q. Tian and X. H. Bao, *Nat. Nanotechnol.*, 2016, **11**, 218–230.
5 H. J. Yin and Z. Y. Tang, *Chem. Soc. Rev.*, 2016, **45**, 4873–4891.
6 T. B. Yuan, Z. Hu, Y. X. Zhao, J. J. Fang, J. Lv, Q. H. Zhang, Z. B. Zhuang, L. Gu and S. Hu, *Nano Lett.*, 2020, **20**, 2916–2922.
7 X. Q. Huang, S. H. Tang, X. L. Mu, Y. Dai, G. X. Chen, Z. Y. Zhou, F. X. Ruan, Z. L. Yang and N. F. Zheng, *Nat. Nanotechnol.*, 2011, **6**, 28–32.
8 H. W. Zhao, Y. J. Zhu, F. S. Li, R. Hao, S. X. Wang and L. Guo, *Angew. Chem., Int. Ed.*, 2017, **56**, 8766–8770.
9 Z. W. Fang, Q. Y. Xing, D. Fernandez, X. Zhang and G. H. Yu, *Nano Res.*, 2020, **13**, 1179–1190.
10 W. R. Cheng, J. F. He, T. Yao, Z. H. Sun, Y. Jiang, Q. H. Liu, S. Jiang, F. C. Hu, Z. Xie, B. He, W. S. Yan and S. Q. Wei, *J. Am. Chem. Soc.*, 2014, **136**, 10393–10398.
11 Z. Q. Sun, T. Liao, Y. H. Dou, S. M. Hwang, M. S. Park, L. Jiang, J. H. Kim and S. X. Dou, *Nat. Commun.*, 2014, **5**, 3813.
12 B. Akram, W. X. Shi, H. Zhang, S. Ullah, M. Khurram and X. Wang, *Angew. Chem., Int. Ed.*, 2020, **59**, 8497–8501.
13 C. Liu, L. R. Zheng, Q. Song, Z. J. Xue, C. H. Huang, L. Liu, X. Z. Qiao, X. Li, K. Y. Liu and T. Wang, *Angew. Chem., Int. Ed.*, 2019, **58**, 2055–2059.
14 C. L. Tan, X. H. Cao, X. J. Wu, Q. Y. He, J. Yang, X. Zhang, J. Z. Chen, W. Zhao, S. K. Han, G. H. Nam, M. Sindoro and H. Zhang, *Chem. Rev.*, 2017, **117**, 6225–6331.
15 G. Xiang, Y. Tang, Z. Liu, W. Zhu, H. Liu, J. Wang, G. Zhong, J. Li and X. Wang, *Nano Lett.*, 2018, **18**, 7809–7815.
16 W. J. Zhao, Y. Huang, C. Shen, C. Li, Y. Q. Cai, Y. Xu, H. T. Rong, Q. Gao, Y. Wang, L. Zhao, L. H. Bao, Q. Y. Wang, G. Y. Zhang, H. J. Gao, Z. Y. Xu, X. J. Zhou and G. D. Liu, *Nano Res.*, 2019, **12**, 3095–3100.
17 H. Z. Zhang and J. F. Banfield, *Chem. Rev.*, 2014, **114**, 9613–9644.
18 M. Kapilashrami, Y. F. Zhang, Y. S. Liu, A. Hagfeldt and J. H. Guo, *Chem. Rev.*, 2014, **114**, 9662–9707.
19 X. G. Han, Q. Kuang, M. S. Jin, Z. X. Xie and L. S. Zheng, *J. Am. Chem. Soc.*, 2009, **131**, 3152–3153.
20 G. L. Xiang, Y. G. Wang, J. Li, J. Zhuang and X. Wang, *Sci. Rep.*, 2013, **3**, 1411.
21 L. Z. Wang and T. Sasaki, *Chem. Rev.*, 2014, **114**, 9455–9486.
22 G. L. Xiang, T. Y. Li, J. Zhuang and X. Wang, *Chem. Commun.*, 2010, **46**, 6801–6803.
23 S. L. Wang, X. Luo, X. Zhou, Y. Zhu, X. Chi, W. Chen, K. Wu, Z. Liu, S. Y. Quek and G. Q. Xu, *J. Am. Chem. Soc.*, 2017, **139**, 15414–15419.
24 P. X. Liu, Y. Zhao, R. X. Qin, S. G. Mo, G. X. Chen, L. Gu, D. M. Chevrier, P. Zhang, Q. Guo, D. D. Zang, B. H. Wu, G. Fu and N. F. Zheng, *Science*, 2016, **352**, 797–801.
25 X. T. Wang, W. X. Shi, S. X. Wang, H. W. Zhao, J. Lin, Z. Yang, M. Chen and L. Guo, *J. Am. Chem. Soc.*, 2019, **141**, 5856–5862.
26 G. L. Xiang, D. Wu, J. He and X. Wang, *Chem. Commun.*, 2011, **47**, 11456–11458.
27 G. P. Neupane, L. L. Zhang, T. Yildirim, K. Zhou, B. W. Wang, Y. L. Tang, W. D. Ma, Y. Z. Xue and Y. R. Lu, *Nano Res.*, 2020, **13**, 1–17.

28 M. S. Xu, T. Liang, M. M. Shi and H. Z. Chen, *Chem. Rev.*, 2013, **113**, 3766–3798.

29 K. Fan, C. Cao, Y. Pan, D. Lu, D. Yang, J. Feng, L. Song, M. Liang and X. Yan, *Nat. Nanotechnol.*, 2012, **7**, 459–464.

30 S. Grimme, *Angew. Chem., Int. Ed.*, 2008, **47**, 3430–3434.

31 K. E. Riley and P. Hobza, *Acc. Chem. Res.*, 2013, **46**, 927–936.

32 K. Müller-Dethlefs and P. Hobza, *Chem. Rev.*, 2000, **100**, 143–167.

33 S. E. Wheeler, *Acc. Chem. Res.*, 2013, **46**, 1029–1038.

34 C. A. Hunter and J. K. M. Sanders, *J. Am. Chem. Soc.*, 1990, **112**, 5525–5534.

35 C. A. Hunter, *Angew. Chem., Int. Ed.*, 2004, **43**, 5310–5324.

36 S. E. Wheeler and J. W. G. Bloom, *J. Phys. Chem. A*, 2014, **118**, 6133–6147.

37 C. D. Sherrill, *Acc. Chem. Res.*, 2013, **46**, 1020–1028.

38 J. Hermann, D. Alfe and A. Tkatchenko, *Nat. Commun.*, 2017, **8**, 14052.

39 C. R. Martinez and B. L. Iverson, *Chem. Sci.*, 2012, **3**, 2191–2201.

40 L. B. Li, R. B. Lin, R. Krishna, H. Li, S. C. Xiang, H. Wu, J. P. Li, W. Zhou and B. L. Chen, *Science*, 2018, **362**, 443–446.